**Title:** Adjustments of global and hindlimb local properties during the terrestrial locomotion of the common quail (*Coturnix coturnix*).

**Authors:** Emanuel Andrada[1], John A. Nyakatura[2], Florian Bergmann[1], Reinhard Blickhan[1]

**Institutions:**

[1]Science of Motion, Friedrich-Schiller University Jena, Seidelstraße 20, 07749 Jena, Germany.

[2]Institut für Spezielle Zoologie und Evolutionsbiologie mit Phyletischem Museum, Friedrich-Schiller-Universität, D-07743 Jena, Germany.

Running title: Global and leg joint dynamics in the quail

**Corresponding author:**

Emanuel Andrada

emanuel.andrada@uni-jena.de

**Keywords:** Avian locomotion, spring-mass, joint control, biomechanics, inverse dynamics, joint stiffness

## Abstract:

Increasing insight into neuro-mechanical control strategies during perturbed locomotion is gained. In contrast, more general analyses on simple model (template) related parameters during avian terrestrial locomotion are still rare. Quails kinematic data obtained using X-ray videography combined with ground reaction force measurements were used as a basis to investigate how "global" template and "local" leg joint parameters in this small predominantly terrestrial bird change with speed and gait. Globally, quail locomotion approximates a spring-like behavior in all investigated gaits. However, ground reaction forces are more vertically oriented which may help to balance the trunk. At the joint level, practically all the spring like work was found to occur in the ITJ (intertarsal joint). From walking to grounded running the local stiffness of the ITJ decreases similarly to the reduction observed in global leg stiffness. Thus, in gaits without aerial phases the quails may modulate ITJ stiffness to regulate global leg stiffness, and therefore gait changes, to a significant degree. At higher speeds both global leg compression and stiffness are increased (the latter to values not significantly different to those obtained during walking). This enables the animals to shorten contact time and to generate aerial phases (running). However, we did not observe a change in the stiffness in the ITJ with a change of gait from grounded running to running. We hypothesize that a more extended leg at touch-down, controlled by the joint angles in knee and ITJ, has an important influence in the leg stiffness adjustment process during running.

## Introduction

When birds increase speed during terrestrial locomotion, they change gait. First, birds change from walking to grounded running (a running gait without aerial phases (Rubenson et al., 2004)). At higher speeds most but not all birds studied so far change from grounded running to aerial running (e.g., Cavagna et al., 1977; Gatesy and Biewener, 1991; Abourachid and Renous, 2000; Rubenson et al., 2004; Nudds et al., 2011; Stoessel and Fischer, 2012). Previous studies have shown that these transitions are often accompanied by i) smooth variations of spatio-temporal parameters as the speed increases (e.g., Gatesy and Biewener, 1991; Abourachid and Renous, 2000 ); ii) gradually increasing leg joint amplitudes with increase of speed (Gatesy and Biewener, 1991; Abourachid and Renous, 2000; Nyakatura et al., 2012; Stoessel and Fischer, 2012), and iii) a gradual shift from vaulting mechanics towards bouncing mechanics of the center of mass (CoM) (Rubenson et al., 2004; Hancock et al., 2007; Nyakatura et al., 2012). Gait changes appear to not always be correlated to changes in the metabolic energy consumption, but specialized walking/running birds utilize specific gaits at given speeds on a treadmill in correlation to energetic minima (Rubenson et al., 2004; Nudds et al., 2011). Although these studies provided important insight into speed related changes of avian terrestrial locomotion, we still know surprisingly little about how global parameters and local parameters at the leg level vary with gait, and thus how their tuning influences gait and motor control strategies.

Global parameters describe biomechanical systems as a whole in the case of terrestrial locomotion by reducing the hindlimb to a "virtual leg" or “global leg” linking the hip or the CoM with the center of pressure (CoP), and by representing the complex action of muscles and tendons by a minimal number of parameters (see below). Such simple models of locomotion are often referred to as templates (Full and Koditschek, 1999). In contrast, assessing local parameters permits inference of each joint’s contribution to global leg behavior. At the global level, the SLIP model (Spring Loaded Inverted Pendulum, also called spring-mass model; Blickhan, 1989) can accurately describe the dynamics of running and hopping, while the BSLIP model (Bipedal Spring Loaded Inverted Pendulum, also called bipedal spring-mass model) can predict those of moderate walking (Geyer et al., 2006; Lipfert et al., 2012) and grounded running (Andrada et al., 2012; Andrada et al., in press), if the appropriate limb parameters for these models are given (limb angle at touch-down, leg stiffness, effective limb length, and for the BSLIP also limb compression).

One of the most investigated global leg parameter is the leg stiffness. Interestingly, studies on speed related changes in leg stiffness during human and animal running leads to contradictory results. In some studies, leg stiffness has been reported to remain constant during running at different speeds both in animals and humans (He et al., 1991; Farley et al., 1993). In contrast, Arampatzis and colleagues (Arampatzis et al., 1999) reported that leg stiffness increase in human running when the speed increased. Experimental evidence shows also that when hopping or running humans encounter sudden

changes in substrate stiffness or damping (Farley et al., 1998; Ferris et al., 1999; Kerdok et al., 2002; Moritz et al., 2004) or changes in terrain height (Grimmer et al., 2008; Müller and Blickhan, 2010), subjects adapt their global leg parameters to the altered situation. For example, on surfaces with lower stiffness, humans increase leg stiffness. The change in leg stiffness is indicated by a reduction in the vertical downwards motion of the CoM from touch-down (TD) to mid-stance and nearly constant maximum leg force (Farley et al., 1998; Ferris et al., 1999; Kerdok et al., 2002). Runners on uneven ground decrease leg stiffness with the increasing height of the vertical perturbation (Grimmer et al., 2008). Here, in contrast to the results obtained on compliant surfaces, change in leg stiffness is more likely to be produced by an altered leg force (Grimmer et al., 2008). In addition, the adaptation of global leg parameters during running on uneven ground seems to exploit the self-stabilizing properties of the SLIP model to stabilize locomotion (Grimmer et al., 2008; Müller and Blickhan, 2010). Valuable experiments on running birds over tracks with unexpected changes of terrain height have also been conducted (e.g. Daley et al., 2006; Daley et al., 2007). Here, the delay in ground contact resulted in a steeper but more variable angle of attack. This effect could be attributed to swing-leg retraction, which can enhance the tolerance to ground disturbances significantly (Seyfarth et al., 2003). Although leg stiffness during the unexpected drop varied dramatically (Daley et al., 2007), it remains unclear how this adjustment of leg stiffness facilitated the continuation of rhythmic striding locomotion. More general information about gait related changes in avian leg stiffness is largely missing. In the present paper we aim to study how global leg stiffness in a small predominantly terrestrial bird changes with speed and gait, and which joints may mainly be responsible in tuning global leg stiffness.

Our first main hypothesis is that at the global leg stiffness may approximate a spring-mass behavior for all gaits. Contrary to humans or large animals which walk with extended legs, and thus with high leg stiffness (for humans see Lipfert et al., 2012), the crouched posture observed in small animals (e.g. Biewener, 1989; Gatesy and Biewener, 1991; Witte et al., 2002; small animals being defined as having a body mass < 1 kg following Biewener, 1989) may enable spring-like locomotion at lower speeds. In particular, we expect that overall low stiffness is highest during walking. Joint angles undergo smaller flexions during walking as compared to running (e.g. Gatesy and Biewener, 1991; Abourachid et al., 2011; Nyakatura et al., 2012; Stoessel and Fischer, 2012). When switching from walking to grounded-running this is considered to be equivalent to a switch from stiff legged vaulting to compliant bouncing. We also expect a transition between grounded running and running to be represented by an increase of both global leg stiffness and global leg compression, to cope with the reduced contact times and to exert higher vertical GRF.

Our second main hypothesis is that the more distal joints (intertarsal joint [ITJ], and the tarsometatarso-phalangeal joint [TMTJ]) are responsible for tuning global leg stiffness, and therefore

play an important role in controlling gait transitions. We base this expectations on the result of previous studies, that have shown in running guinea fowl the more distal joints may act as spring-like elements, while more proximal ones (hip, knee) did not show energy storage during either level running (Daley and Biewener, 2003) or unexpected drops (Daley et al., 2007). Similarly, Rubenson and colleges showed that ostrich store and release elastic energy mainly in the TMTJ (Rubenson et al., 2010). In humans, Kuitunen and colleagues (Kuitunen et al., 2002) observed increments in the knee stiffness with increasing running speed. Others (Farley and Morgenroth, 1999; Müller et al., 2010) reported that leg stiffness during hopping and running over uneven terrain seems to depend mostly on ankle stiffness. In order to test our second hypothesis we expect correlation between the changes observed in the global stiffness with those observed at the joint level.

We investigate this by combining kinematic data derived from X-ray motion analysis with single limb force plate measurements during the locomotion of the common quail. This permits us to evaluate both the virtual leg function during stance (CoP-CoM), and joint mechanics by using inverse dynamics analysis and joint kinematics.

## Material and methods

### *2.3.1 Animals*

Eight adult common quails (Phasianidae: *Coturnix coturnix*, Bonnaterre 1791) weighing between 180 g and 240 g were obtained from local breeders. The birds were housed in spacious cages with access to food and water *ad libitum*. The Committee for Animal Research of the State of Thuringia, Germany, approved the animal care and all experimental procedures (registry number: 02-47/10).

### *2.3.2 X-ray motion analysis*

The birds moved across a 3 m long walking-track at their preferred speeds. The track was covered with fine sand paper (grit 40) to reduce slipping. We simultaneously recorded kinematics and ground reaction forces (GRFs). For the kinematic analysis, synchronized, biplanar X-ray videography (Neurostar, Siemens®, Erlangen, Germany) at the facility of the Institut für Spezielle Zoologie und Evolutionsbiologie mit Phyletischem Museum, Germany was used. X-ray recordings were taken from the latero-lateral and ventro-dorsal projections. Due to the limited size of the image intensifiers only 38 cm of the track (including the instrumented part - see below) were visible in the X-ray recordings. Our experimental setup additionally had two synchronized standard light high-speed cameras (SpeedCam Visario g2, Weinberger®, Erlangen, Germany) filming from a frontal and lateral perspective to cover a larger portion of the track. The X-ray machine operated at 40 kV and 53 mA,

147 with a sampling frequency of 1 kHz. We filtered the raw video data (e.g., gamma correction, contrast,
148 sharpness) and, finally, performed the digitization of the joints and other landmarks (Fig. 1A) using
149 SimiMotion® software (SimiMotion Systems, Unterschleißheim, Germany). X-ray videos suffer from
150 distortion and were therefore corrected prior to analysis with use of a freely available MATLAB® (the
151 Mathworks Inc., Natick, MA, USA) routine (www.xromm.org) provided by Brown University
152 (Providence, USA).

153

154 *2.3.3 Force data acquisition and analysis*

155 We measured three-dimensional GRFs (ground reaction forces) and CoP (center of pressure) with two
156 custom-built (8 cm x 9 cm) force plates, which we integrated into the walking-track. In order to
157 reduce metal parts in the area of the X-ray beams, we used carbon fiber to construct the force plates
158 and their support. We used 6-DOF (degree of freedom) force-torque sensors (ATI nano17®) as
159 transducer elements. Using fast Fourier transformation, we measured the plates' dominant
160 eigenfrequency, which turned out to be above 200 Hz. Furthermore, our static tests revealed the
161 resolution of the CoP position to be below 1 mm at loads higher than 300 mN. According to the
162 sampling rate of the kinematic data, we collected ground reaction forces at 1 kHz (NI USB-6229,
163 National Instruments®; custom software LabView 2009 National Instruments®). We synchronized
164 force and X-ray analysis electronically (post-trigger).

165

166 *Determination of limb element and body part properties*

167 One of the individuals (subject 6) was sacrificed and dissected. Limb elements were detached
168 at the joints and body elements (torso, head, and neck) were dissected from each other. We then
169 weighed each element and used a pendulum method to determine each element's CoM position as
170 described in (Nyakatura et al., 2012) (Table 2). Elements were defined using landmarks which are
171 easy to identify in the x-ray films (Fig. 1A), and the position of the element's CoM is presented as %
172 of element length measured from the proximal landmark (Table 1). The following elements and body
173 parts were defined (from proximal to distal or cranial to caudal landmarks, respectively): thigh (femur
174 proximal to femur distal), tibiotarsus (tibiotarsus proximal to tibiotarsus distal), tarsometatarsus
175 (tarsometarsus proximal to tarsometatarso-phalangeal joint), toes (tarsometatarso-phalangeal joint to
176 tip of middle toe), trunk including the wings (from caudalmost cervical vertebra to pygostyl), neck
177 (occiput to caudalmost cervical vertebra), head (tip of beak to occiput). For toes and tarsometatarsus
178 the position of the CoM was assumed to be at half the length of these cylindrical elements. We also
179 assumed a fixed CoM position between the two landmarks defining the neck, to account for the
180 constant changes of its length due to movements of the head relative to the trunk. We used linear

transformation of the data of the sacrificed subject to estimate the element parameters of the other subjects in accordance to a subject's overall weight.

*Mechanics of the center of mass*

To distinguish between walking and grounded running, it is necessary to assess the fluctuations of gravitational potential energy ($E_p$) and kinetic energy ($E_k$) of the body's CoM due to the gradual shift of kinematic parameters between both gaits (Gatesy and Biewener, 1991; Stoessel and Fischer, 2012). Moreover, it has been demonstrated that terrestrial locomotion in small birds rarely approaches the ideal cases of either in-phase or out-of-phase fluctuation of both energy forms ( e.g. Hancock et al., 2007; Nyakatura et al., 2012) as proposed to define walking and running mechanics (e.g. Cavagna et al. 1977; Heglund et al., 1982; Blickhan and Full, 1992). For the purposes of this study we categorized all trials to either walking, grounded running, or running. We relied on the percentage of congruity, as proposed by (Ahn et al., 2004), between $E_p$ and $E_k$ to discriminate running from walking. This parameter more closely compares the form of the graphs for $E_p$ and $E_k$ and therefore was suggested to better reflect the phase relationship than a mere comparison of the local minima as in the calculation of phase shift. %Congruity is calculated using the product of instantaneous changes (here video frames) between $E_p$ and $E_k$. All cases of a product greater than zero, that is, when the two energies are congruent, are summed and reported as the percentage of overall frames. Ideally, %Congruity would be 100% in a running trial and 0% in a walking trial. We defined walking for %Congruity values < 50 and running for %Congruity values > 50. For values close to 50% we further analyzed the shape and value of the GRF, and vertical speed change of CoM at mid-stance (anterior-posterior GRF, Fx = 0). In running, i.e. bouncing mechanics, the CoM's vertical speed changes from negative to positive at mid-stance. For symmetric steady-state walking, vertical GRF has to be lower than body weight (1 BW) at mid-stance (M-shape), and CoM's vertical speed changes from positive to negative at mid-stance, i.e. vaulting mechanics. We are aware of the fact that asymmetries as usually observed in animal locomotion will slightly shift the local extremes of the force patterns and thus the transition speed.

We calculated the instantaneous position of the body's CoM from kinematic data (X-ray motion analysis data of the limbs, additional kinematic data of digitized head, neck and torso landmarks, and each element's CoM position). To validate the kinematic analysis, we also determined the CoM trajectory by double integration of the anterior-posterior and vertical accelerations ($a_x$; $a_y$) obtained from the measured GRF divided by body mass. As initial position of the CoM ($s_{0x}$; $s_{0y}$) we used those obtained kinematically. As kinematic methods do not account for movement of appendages and viscera, kinematically determined CoM initial speeds ($v_{0x}$; $v_{0y}$) are imprecise to be used as integration constants. Thus, we optimized CoM initial speeds' estimates by minimizing the sum of squared distances between the kinematically determined CoM trajectory and CoM trajectory derived from

force plate analysis as described in (Daley et al., 2007). For locomotion close to steady-state, both methods match (Fig. 2A).

*2.3.4 Global and local leg stiffness*

The global analysis is based on the BSLIP template (Geyer et al, 2006). The BSLIP model consists of the body as a point mass $m$ at the CoM and two massless, linear springs with a given stiffness $k$ and rest length $l_0$ describing the action of the legs during stance. Each spring acts independently, and the swing phase is used to adjust the angle of attack $\alpha_0$ related to the ground or the aperture angle $\phi_0$ related to the stance leg (Fig. 1D). Motion is restricted to the sagittal plane, hence the equations of motion of the CoM are:

$$m\ddot{x} = -k(l_0 - l_1)\cos\alpha_1 - k(l_0 - l_2)\cos\alpha_2 \qquad (1)$$

$$m\ddot{y} = -mg + k(l_0 - l_1)\sin\alpha_1 + k(l_0 - l_2)\sin\alpha_2 \qquad (2),$$

where $\ddot{x},\ddot{y}$ are the accelerations of the CoM, $m$ is the body mass, $g$ is the gravitational acceleration, $l_1$ and $l_2$ are the instantaneous leg lengths during stance, and $\alpha_1$ and $\alpha_2$ are the corresponding orientations between the ground and each leg. In the single-support phase, only one leg exerts force and the last right-hand term in both equations is zero, whereas in the double-support phase both legs exert force and hence, all right-hand terms in both equations are nonzero. During aerial phases, the trajectory of the center of mass is influenced only by the gravitational force.

To estimate the global leg stiffness $k$ from experimental data, we computed first the instantaneous virtual leg length as the distance between CoM and CoP. As virtual leg length is normally non-symmetrical relative to touch-down (TD) and take-off (TO) events, we averaged relative virtual leg lengths in order to determine the global leg stiffness $k$ from kinetic data. We computed $k$ as $k = GRF_{mid-stance} / \Delta l$, where $\Delta l = (l_{leg\_TD} + l_{leg\_TO}) / 2 - l_{leg\_mid-stance}$. Note that $l_0 = (l_{leg\_TD} + l_{leg\_TO}) / 2$ is the rest length of the assumed spring (Fig. 3). This approach assumes that the virtual leg behaves like a linear spring. To enable comparison with other species we present global and local parameters in dimensionless form, following Andrada and co-workers (Andrada et al., 2012; Andrada et al., in press). Dimensionless global leg stiffness was defined as $\hat{k} = kl_0 / mg$, where $m$ is the mass of the bird and $g$ gravity. The dimensionless global leg compression ($\psi$) related to the compression of the spring at mid-stance is equal to the GRF in body weight ($\psi = GRF / mg = k(l_0 - l) / mg$; see Andrada et al., 2012; Andrada et al., in press).

We determined the angle of attack at touch-down ($\alpha_0$) between the ground and the segment CoM-CoP as shown in Fig. 1C, and the aperture angle $\phi_0$ at touch-down, following Andrada and colleagues (Andrada et al., in press), by computing the angle between the CoPs of the stance legs and the CoM

(Fig. 1C). We measured limb segmental angles related to the ground, and joint angles as shown in Fig. 1B.

Global leg properties must be generated locally at the joint level. Calculation of local stiffness requires estimates of joint torques. We estimated torque at each joint during stance using a quasi-static analysis neglecting segment inertia and weight. Especially during slow locomotion, the error in estimating joint torques from GRF should be negligible (as linear and rotational accelerations are low). Moreover, Witte and co-workers showed that for small mammals even during fast locomotion the inertia of the extremities only contribute a maximum of 10% to overall forces (Witte et al., 2002). In our case, even at the maximal running speed measured, the influence of femur segment`s moment of inertia to the joint torque, estimated as a thin rod $J_f\ddot{\theta}_f = \frac{m_f l_f^{\,2}}{3}\ddot{\theta}_f$, is lower than 5% of the maximal observed torque (cp. Fig. 7). Here, $J_f$ represents the moment of inertia, $l_f$ the length, and $m_f$ the mass of the femur (see Table 1). $\ddot{\theta}$ represents the maximal angular acceleration of the segment measured during running (800 $1/s^2$). Thus, external torque was computed as the magnitude of the cross product between the instantaneous joint position vector relative to the position of the CoP, and the instantaneous GRF vector P (KNEE and ITJ instantaneous joint positions were assumed to be located in the middle between the distal and proximal ends of adjacent bones; while HIP and TMTJ joints were assumed to be located at the proximal tip of the femur and the distal tip of the tarso-metatarsus, respectively).

*Data analysis*

For final data analysis we were able to obtain a total of 74 steady-state strides (32 walking, 34 grounded running, and 8 running) of biplanar X-ray recording and synchronous, single limb SRF traces. For our investigation of steady- state locomotion we discarded all trials with a horizontal speed deviation of more than 5 % during stance. Trials fulfilling this criterion were the exception. About 10 trials were necessary to obtain a single steady-state trial with both feet not overstepping one of the plates. In most cases these successful trials were grounded runs or walking trials, while aerial running was rarely used by the quails (note that in previously published treadmill studies quails never ran using aerial phases; cf.(Gatesy and Biewener, 1991; Stoessel and Fischer, 2012)). We used t-test to determine whether maximal joint torques, linear and rotational stiffness are gait related (significance level $p < 0.05$) in SPSS 18 (IBM, Armonk, NY, USA).

*Simulations*

Subsequently, we performed BSLIP forward simulations using the mean values of the global parameters obtained experimentally to test for differences between observed data and the linearity assumptions of the BSLIP. We compared GRFs, leg length variation, and contact time from both experimental and BSLIP results during walking, grounded running and aerial running. For walking

and grounded running simulations started at mid-stance ($x_0$ = 0 and $v_{0y}$ = 0). Running simulation started at the *apex* ($y_{max}$, $x_0$ = 0, $v_{0y}$ = 0). $v_{0x}$, $k$, $l_0$, and, $\phi_0$ or $\alpha_0$ were set according to the experimental data, while the initial high $y_0$ was set to match best possible the value of the GRF/$mg$ = $\psi$ at mid-stance. For walking and running, we applied the commonly used angle of attack as TD strategy. For grounded running the aperture angle between legs was preferred (following Andrada et al., 2012; Andrada et al., in press).

Applying the fixed aperture angle $\phi_0$ between legs, the touch-down of the swing leg occurs when $y = l_0 \, sin(\alpha - \phi_0)$, where $\alpha$ is the instantaneous stance leg angle with respect to the ground measured clockwise (Fig. 1D). In contrast, using the fixed angle of attack $\alpha_0$, touch-down of the swing leg occurs when $y = l_0 \, sin\alpha_0$. Take-off occurs when the spring force becomes zero. During running we ensure that only one leg can land at a time. We implemented the simulation model in MATLAB/SIMULINK® (The MathWorksInc., Natick, MA, USA). To integrate eq. 1) and 2) we applied a Runge–Kutta variable-step algorithm (ode45) with a relative and absolute integrator error tolerance of 1e-9.

## Results

Walking was observed at speeds ranging from 0.15 m/s to 0.51 m/s with a mean of 0.34 m/s, grounded running at speeds between 0.42 m/s and 0.79 m/s with a mean of 0.58 m/s, and aerial-phase running gaits were observed at speeds ranging from 0.75 m/s to 1.56 m/s with a mean of 1.06 m/s. The walking-grounded running transition showed a speed overlap of 0.09 m/s. Grounded running-running transition seems to be more defined (just one running trial overlapped with grounded running speeds, Fig. 2B).

The vertical component of the GRF we obtained for the quails displayed the well-known M-shape for walking, a positive skewed half-sine pattern for grounded running, and a less skewed half-sine shape for running (Fig. 4). Notably, at very slow walking the vertical component of the GRF displayed a three peaks shape, as predicted by the BSLIP model (Geyer et al., 2006) but uncommon in human bipedalism (Fig. 5). Anterior-posterior GRFs approximated negative sine-waves for the different gaits.

*Gait related changes in global parameters*

The asymmetry of the virtual leg length between TD and TO events increased with the speed (Fig. 4). While the angle of attack was not significantly different between gaits, the aperture angle varied significantly between walking and grounded running (Table 2). The value $l_0$, associated with the rest length of the spring in the (B)SLIP model, was similar for walking and grounded running, but significantly longer for running (Table 2). Leg stiffness decreased significantly from walking to grounded running and increased again significantly at running gaits. Interestingly, leg stiffness during

walking and running did not differ significantly, while global leg compression increased with speed and was significantly different between gaits (Table 2). Our findings show two important deviations between experimental data and (B)SLIP model assumptions. The first is that GRF are not directed to the CoM as expected for the (B)SLIP model, but more vertically oriented. The second difference from the SLIP is shown by the fact that CoP is shifted cranially during stance. It starts approximately halfway between the tarsometatarso-phalangeal joint (TMTPJ) and tip of the middle toe (ToMT) and moves cranially up to the ToMT during stance (Fig. 6). Nevertheless, simulation results match surprisingly well the quails' leg length variation displayed during walking, grounded running, and aerial running. GRF profiles display more marked differences. These are, for grounded and aerial running, mostly related to the symmetry of the BSLIP model. In case of walking the M-shape of the simulated vertical GRF almost disappears, due to the spring-leg compression at mid-stance (Fig. 4). Contact times calculated in the simulation during walking and grounded running are below those obtained experimentally (w.: 15% less and g.r.: 25% less), while those observed and calculated for running agree (Table 2). Moreover, double support phases, expressed as percent of the stance time, are overestimated in simulations (experimentally: w.: 25% and g.r.: 21%; simulation: w.: 39% and g.r.: 23 %).

*Gait related changes in local parameters*

*Joint angles* displayed similar angle profiles in all gaits. Except for the tarsometatarso-phalangeal joint all other joints were more extended at TD with increasing speed (walking, grounded-running, running) (Fig.7). The *hip joint* underwent a gravity induced flexion at TD as body weight was shifted to the supporting leg. Then it was extended until the end of the stance phase. The *knee joint* was flexed until ca. 60% of stance, and then flexion was kept constant up to 90% of stance. In gaits with double support the knee was then further flexed until TO. The *intertarsal joint* was flexed in the early stance phase, and then extended up to 90% of stance, where the joint was again flexed until TO in the gaits with double support. Interestingly, both knee and intertarsal joints start with the same joint angle in each gait. The *tarsometatarso-phalangeal joint* was flexed in all gaits until ca. 85% of stance and afterwards extended quickly.

In Fig. 7 *joint external torques* during stance estimated for walking, grounded running, and running are presented. In the knee joint a sinusoidal torque pattern was observed, i.e. the torque alters sign during stance and must be compensated by flexors in the first half of the stance and then by extensors. All other joints presented a half-sine torque time relationship and must be compensated by anti-gravitational extensors moments.

While transitioning from walking to grounded running, maximal joint torques increased significantly only for the hip and intertarsal joints. When comparing grounded running with running, maximal joint torques increased significantly for all joints with the most significant increment in the knee joint (61.6 %, Table 3).

The torque-angle loops for each joint are presented in Fig. 7. The intertarsal joint was the only joint

which displayed linear-like torque-angle relation at each gait, as expected for a rotational spring ($M = k\theta$). Following the changes observed for the global stiffness, the rotational stiffness in the intertarsal joint decreased significantly from walking to grounded running. But between grounded running and running, it did not change (see table 3).

## Discussion

The first goal of this paper was to analyze whether variations in leg stiffness in quail, a representative small terrestrial bird, relates to the predictions of the (B)SLIP model, when they change gait as speed increases. The second goal was to infer the contribution of each joint to the global spring-like behavior of the legs in these small birds.

### *Global parameters related to the SLIP and BSLIP model*

When quails switch gait from walking to grounded running or from grounded running to running, they roughly adapt leg stiffness following the (B)SLIP model. As expected, global leg stiffness in quails decreases when they change from vaulting to bouncing mechanics, and increases again during bouncing mechanics as they increase speed. Deviations from a Hookean (linear) spring are obvious especially during walking (Fig.4 right side, above). Nevertheless, our experimental and simulation results indicate that these small birds' locomotion approximates spring-like leg behavior in all gaits. This includes slow walking speeds, at which we obtained three peaks in the shape of the vertical GRF trace, which until now were only predicted by simulations (Geyer et al., 2006).Contrarily, in walking humans strong deviations occur from the spring-like leg behavior (Lipfert et al., 2012). Small birds walk and run with a more crouched posture favoring a compliant leg behavior ( Gatesy and Biewener, 1991; Andrada et al., 2012; Stoessel and Fischer, 2012; this paper). Although torques are relatively higher for crouched legs, the demand for high speed and/or acceleration distance per step, i.e., high locomotor performances (Günther et al., 2004), or the need to cope with rough terrain (Daley and Usherwood, 2010; Birn-Jeffery and Daley, 2012; Andrada et al., in press), may be criteria enforcing such a leg configuration. In humans or other larger animals, swing leg inertia and decrease of effective mechanical advantage (ratio of the extensor muscle moment arm to the moment arm of the GRF; Biewener, 1989) prevent such postures during locomotion, and grounded running is mostly avoided. Accordingly, higher stiffness and more extended legs are observed (e.g., humans $\hat{k} > 40$ (Lipfert et al., 2012) *vs.* $\hat{k} \cong 6$ in quails at comparable Froude numbers representing walking). The weight of the body induces an almost seven times higher compression in a quail than in a human. Interestingly, quails seem to use the same global leg stiffness during walking and running. Certainly, the more extended leg (increased $l_0$) in running is one of the factors which produced an increase of the dimensionless global leg stiffness (see *joint stiffness vs. global leg stiffness*). In a system dominated by the series compliance of passive structures the possibilities of actuators to increase stiffness are largely

reduced. This may be one of the reasons why quails, and probably other small birds, do not usually use aerial running gaits, favoring instead grounded running.

While the angle of attack remains unaltered over the three gaits, in gaits with double contact phases, the aperture angle seems to be a variable that is tuned (Andrada et al., in press). Theoretical models show that grounded running simulated with an aperture angle strategy is less unstable and less sensitive to inaccuracies in angle tuning than the same model simulated with the angle of attack (Andrada et al., 2012; Andrada et al., in press).

Contrarily to the expectation of the spring-mass model, in which the vectors of the GRF always point to the CoM, our results show more vertically oriented forces. This vertical orientation is likely to be produced by hip torques necessary to balance the trunk. In simulations Maus and colleagues did show, that if GRF are directed to a point located above the CoM during stance, trunk posture can be stabilized (Maus et al., 2010). In addition a more vertical oriented GRF may result in reduced energy consumption, as elegantly presented by Usherwood and Hubel (2012). In running, torques about the CoM during stance can—with nonzero body pitch moments of inertia—reduce the mechanical work of supporting body weight by reducing horizontal forces, and thus fore–aft energy fluctuations (Usherwood and Hubel, 2012). The additional cost of balancing the trunk may be compensated for by a reduced cost to drive the energy fluctuations of the CoM.

We are aware that our method for determining stiffness (see methods and Fig. 3), especially during walking, may underestimate this parameter as non-linearities increase. Yet this method is easy to be implemented as just the vertical component of the GRF is needed. Moreover, in a different stance time leg force is overestimated as it does not point to the CoM (Fig. 6). Finally, our simulations match the quails' leg length variation and contact times reasonably well. Higher stiffness values using the linear BSLIP template would certainly diminish matching of those parameters.

*Joint torques*

Net limb joint torques in humans and quadrupedal mammals generally reflect the need to counteract gravity (Winter, 1995; Witte et al., 2002; Nyakatura and Andrada, 2013). Necessary extensor torques result from the 'anti-gravity role' of limb joint extensors to prevent gravity induced limb collapse during weight bearing (Cohen and Gans, 1975; Jenkins and Weijs, 1979; Goslow et al., 1981). With the only exception of the knee, which shows a biphasic torque pattern, external torque results obtained for hip, ITJ, and TMTJ in the quail agree with these observations. Knee torques and joint angles estimated for walking, grounded running and running indicate that the knee is actively flexed from TD until after mid-stance by the knee flexors and not only by gravity (Fig. 7). The change from flexor to extensor moment occurs earlier as the speed increases. Thus, the active flexion of the knee may contribute to body propulsion. After mid-stance, the extensor torque in the knee may work against

gravity, while the hip adopts the role of body propulsion as soon as the vector of the GRF is pointed behind the CoM. Interestingly, Stoessel and Fischer (2012) showed that when speed is increased, the relative kinematic contribution of the knee to the step decreases while that of the hip and ITJ increases. These results agree to some degree with the kinematic notion, that striding bipedalism in extant birds at slow speeds may be characterized as knee-driven (e.g. Gatesy, 1999; Hutchinson and Allen, 2009). The knee-driven mechanism is often linked to a more cranially positioned CoM and a more horizontal oriented femur (Gatesy, 1999; Hutchinson and Allen, 2009) in birds in comparison with humans.

The increased knee flexion observed may be explained by the action of the biarticular *M. gastrocnemius* in combination with the bird specific leg geometry. In birds, the lateral gastrocnemius muscle (LG) solely flexes the knee (Higham et al., 2008). The crouched posture increases the moment arm of this muscle. Consequently, the knee joint is more susceptible to flexion from flexor muscle activity. To antagonize this effect in the late stance, the modulation of the joint stiffness has to be achieved by knee extensor muscles, as for example, the medial part of the gastrocnemius muscle (MG; see below and (Higham et al., 2008)), *M. femoro-tibialis* or *M. ilio-tibialis*. Flexor knee torques in the early stance phase were also observed in running guinea fowl (Daley et al., 2007) and ostriches (Rubenson et al., 2010). Ostriches have more extended legs, and the knee is only flexed until ca. 20% of the stance followed by a strong extension (see Rubenson et al., 2007, Rubenson et al., 2010). In human locomotion depending on the knee joint angle, the MG may act as a knee flexor or as a knee extensor (Ertelt et al., 2011). At knee joint angles between 150° and 180° Ertelt et al., 2011 observed that the MG works as a knee extensor, but below 150° the contraction of this muscle will work against knee extension. Thus, the extended leg in humans prevents the knee flexing action of MG and it may even extend the knee. Contrarily, the medial head of the avian gastrocnemius generally wraps right around the knee and is a knee extensor even at flexed knee angles (Higham et al., 2008). However, the insertions of the LG and MG act about the ankle joint via a common tendon. Thus, the contraction of both parts of *M. gastrocnemius* extends the ITJ joint, for which - together with the hip joint - we found the biggest extensor torques.

Our findings show that, on average, bouncing leg behavior demands significant higher torques in the hip (13.0%) and intertarsal (18.7%) joints in respect to vaulting leg behavior. These increments, however seem to be relative moderate if we take into account that the speed increased between these two gaits on average by about 70%. Obviously, grounded running offers the advantage of long step lengths and contact times, increasing the distribution of ground reaction forces. The result is a reduction in peak reaction forces and thus joint torques compared to gaits which feature greater limb stiffness and/or aerial phases. Energy storage and the reduction in peak force in grounded running may thus help to reduce the cost of locomotion. In contrast, the decrease in the effective mechanical advantage of the musculature may cancel out this effect (McMahon et al., 1987; Biewener, 1989).

When quails run with aerial phases maximal joint torques increase significantly. Our results show that the most important relative increment occurs, surprisingly, in the knee joint. This is likely to be produced, by the significant increased force generated by the LG during running (Higham et al., 2008) needed to cope with higher flexing moments in the ITJ joint.

*Joint stiffness vs. global leg stiffness*

We hypothesized the intertarsal joint (ITJ) and the tarsometatarso-phalangeal joint (TMTJ) to be responsible in tuning global leg stiffness. Contrarily to our assumptions, the TMTJ did not display quasi-linear torque-angle relation, as expected for a rotational spring. This was only observed for the intertarsal joint. The latter can largely explain the changes observed for the global leg stiffness between walking and grounded running. Comparing the mean values of each gait presented in tables 2 and 3, the rotational stiffness in the intertarsal joint decreased about 20% while the overall leg stiffness decreased about 14%. On the other hand, the ITJ stiffness estimated for running did not differ from those obtained for grounded running, while the leg stiffness increased about 23% between these two gaits. This may indicate that the ITJ changes gradually between two behaviors, namely vaulting and bouncing. The observed increase may also be a cumulative result of the action of non-linearities among leg joints. The more extended leg is one of the factors which produced an increment of the dimensionless leg stiffness. First, the observed $l_0$ increase (about 8%) can explain partially the increase of 20% in the dimensionless leg stiffness between these gaits. The second component may be the result of a more extended knee. Farley and colleges discussed that the ankle stiffness is affected by the knee angle at TD which changes the activation of the *M. gastrocnemius*, *M. tibialis anterior* or *M. soleus* (Farley et al., 1998). Thus a more extended knee, as observed in our results, may result in an increase in *M. gastrocnemius* force without necessity of changes in the activation of that muscle (Müller et al., 2010). In addition, the more extended leg during running increases the effective mechanical advantage (Biewener et al., 2004). If activation is not altered, this results in an automatic increment in leg stiffness (Blickhan et al., 2007). Therefore, our results indicate that an important part of the leg stiffness adjustment process may rely on the leg geometry at TD, as already hypothesized (Grimmer et al., 2008; Müller and Blickhan, 2010). In this respect, morphological, electromyography (EMG) as well simulation studies are needed to understand how leg geometry and joint non-linear behavior contributes to a linear-like leg stiffness.

## Conclusion

Quail terrestrial locomotion globally approximates a linear-like spring-like behavior at all investigated gaits (walking, grounded running, and running), correlated with the predictions of the (B)SLIP model. This includes slow walking which is characterized by a three hump curve in the vertical GRF, as predicted by the BSLIP (Geyer et al., 2006). Trunk balance during all gaits seems to be an important issue and thus GRFs are, contrarily to the telescopic expectation of the (B)SLIP model, more vertically oriented. As previously observed, swing leg behavior is highly conserved during all gaits (e.g., Gatesy and Biewener, 1991; Nyakatura et al., 2012; Stoessel and Fischer, 2012), while the retraction of the stance leg (e.g., Gatesy and Biewener, 1991; Nyakatura et al., 2012; Stoessel and Fischer, 2012), and therefore the aperture angle (Andrada et al., 2012; Andrada et al., in press) is adapted as speed increases. At the local level, practically all the spring like work was found to occur in the ITJ, while the active knee flexion is more likely to help in the regulation of the leg retraction. Contrarily to the results from Rubenson and colleagues (Rubenson et al., 2010) from ostriches, the TMTPJ in quails displayed no spring-like behavior. This may highlight a difference between large and small birds. Finally, our results show that between walking and grounded running the stiffness in the ITJ decreases in a similar way to the diminution observed in the global leg stiffness. Thus, in gaits without aerial phases the ITJ stiffness significantly regulates overall leg stiffness. Accordingly, global leg compression increased to exert higher vertical GRFs at mid-stance during grounded running compared to walking.

Higher global leg compression and thus higher leg forces permits quails to introduce aerial phases, and leg stiffness is increased (to values which are not significantly different to those obtained during walking) to cope with the decreasing contact times. However, the stiffness in the ITJ does not change from grounded running to running. Here, the more extended leg at TD adds to the notion that an important part of the leg stiffness adjustment process in running may rely on the leg geometry at TD, controlled by the joint angles in knee and ITJ.

**Acknowledgments:** We thank Roy Müller for stimulating and helpful discussions that lead to the first manuscript of this work. We thank our colleagues Vivian Allen, Brandon Kilbourne, and Alexander Stoessel for providing helpful critique on early drafts of the manuscript. Rommy Petersohn and Ingrid Weiß helped with X-ray data acquisition. Three reviewers' comments helped to improve and clarify the manuscript. Figure 3 is based on a sketch provided by Rev.#3 and the Editor (AA Biewener). This research was supported by DFG (German Research Council) grants Bl 236/22-1 and Fi 410/15-1.

## References:


**Abourachid, A. and Renous, S.** (2000). Bipedal locomotion in ratites (Paleognatiform): examples of cursorial birds. *Ibis* **142**, 538-549.

**Abourachid, A., Hackert, R., Herbin, M., Libourel, P. A., Lambert, F., Gioanni, H., Provini, P., Blazevic, P. and Hugel, V.** (2011). Bird terrestrial locomotion as revealed by 3D kinematics. *Zool* **114**, 360-368.

**Ahn, A. N., Furrow, E. and Biewener, A. A.** (2004). Walking and running in the red-legged running frog, Kassina maculata. *J Exp Biol* **207**, 399-410.

**Andrada, E., Rode, C. and Blickhan, R.** (in press). Grounded running in quails: simulations indicate benefits of observed fixed aperture angle between legs before touch-down. *J Theor Biol*.

**Andrada, E., Nyakatura, J. A., Müller, R., Rode, C. and Blickhan, R.** (2012). Grounded Running: An Overlooked Strategy for Robots. In *Autonomous Mobile Systems 2012*, pp. 79-87: Springer Berlin Heidelberg.

**Arampatzis, A., Bruggemann, G. P. and Metzler, V.** (1999). The effect of speed on leg stiffness and joint kinetics in human running. *J Biomech* **32**, 1349-1353.

**Biewener, A. A.** (1989). Scaling body support in mammals: limb posture and muscle mechanics. *Science* **245**, 45-48.

**Biewener, A. A., Farley, C. T., Roberts, T. J. and Temaner, M.** (2004). Muscle mechanical advantage of human walking and running: implications for energy cost. *J Appl Physiol* **97**, 2266-2274.

**Birn-Jeffery, A. V. and Daley, M. A.** (2012). Birds achieve high robustness in uneven terrain through active control of landing conditions. *J Exp Biol* **215**, 2117-2127.

**Blickhan, R.** (1989). The spring-mass model for running and hopping. *J Biomech* **22**, 1217-1227.

**Blickhan, R. and Full, R.J.** (1992). Mechanical work in terrestrial locomotion. In: *Biomechanics - Structures and Systems* (ed. AA Biewener). Oxford University Press. Pp: 75-96

**Blickhan, R., Seyfarth, A., Geyer, H., Grimmer, S., Wagner, H. and Gunther, M.** (2007). Intelligence by mechanics. *Philos Transact A Math Phys Eng Sci* **365**, 199-220.

**Cavagna, G. A., Heglund, N. C. and Taylor, C. R.** (1977). Mechanical work in terrestrial locomotion: two basic mechanisms for minimizing energy expenditure. *Am J Physiol* **233**, R243-261.

**Cohen, A. H. and Gans, C.** (1975). Muscle activity in rat locomotion: movement analysis and electromyography of the flexors and extensors of the elbow. *J Morphol* **146**, 177-196.

**Daley, M. A. and Biewener, A. A.** (2003). Muscle force-length dynamics during level versus incline locomotion: a comparison of in vivo performance of two guinea fowl ankle extensors. *J Exp Biol* **206**, 2941-2958.

**Daley, M. A. and Usherwood, J. R.** (2010). Two explanations for the compliant running paradox: reduced work of bouncing viscera and increased stability in uneven terrain. *Biol. Lett.* **6**, 418-421.

**Daley, M. A., Felix, G. and Biewener, A. A.** (2007). Running stability is enhanced by a proximo-distal gradient in joint neuromechanical control. *J Exp Biol* **210**, 383-394.

**Daley, M. A., Usherwood, J. R., Felix, G. and Biewener, A. A.** (2006). Running over rough terrain: guinea fowl maintain dynamic stability despite a large unexpected change in substrate height. *J Exp Biol* **209**, 171-187.

**Ertelt, T., Ertelt, H. J. and Blickhan, R.** (2011). The Geometry-Critical Functional Dependence of M. Gastrognemius. *Int J Appl Mech* **03**, 85-98.

**Farley, C. T. and Morgenroth, D. C.** (1999). Leg stiffness primarily depends on ankle stiffness during human hopping. *J Biomech* **32**, 267-273.

**Farley, C. T., Glasheen, J. and McMahon, T. A.** (1993). Running springs: speed and animal size. *J Exp Biol* **185**, 71-86.

**Farley, C. T., Houdijk, H. H. P., Van Strien, C. and Louie, M.** (1998). Mechanism of leg stiffness adjustment for hopping on surfaces of different stiffnesses. *J Appl Physiol* **85**, 1044-1055.

**Ferris, D. P., Liang, K. and Farley, C. T.** (1999). Runners adjust leg stiffness for their first step on a new running surface. *J Biomech* **32**, 787-794.

**Full, R. J., Koditschek, D. E.** (1999). Templates and anchors: neuromechanical hypotheses of legged locomotion on land. *J. Exp. Biol*. **202**, 3325-3332.
**Gatesy, S. M.** (1999). Guineafowl hind limb function. I: Cineradiographic analysis and speed effects. *J Morphol* **240**, 115-125.
**Gatesy, S. M. and Biewener, A. A.** (1991). Bipedal locomotion: effects of speed, size and limb posture in birds and humans. *J Zool* **224**, 127-147.
**Geyer, H., Seyfarth, A. and Blickhan, R.** (2006). Compliant leg behaviour explains basic dynamics of walking and running. *Proc. R. Soc. B* **273**, 2861-2867.
**Goslow, G. E., Seeherman, H. J., Taylor, C. R., McCutchin, M. N. and Heglund, N. C.** (1981). Electrical activity and relative length changes of dog limb muscles as a function of speed and gait. *J Exp Biol* **94**, 15-42.
**Grimmer, S., Ernst, M., Günther, M. and Blickhan, R.** (2008). Running on uneven ground: leg adjustment to vertical steps and self-stability. *J Exp Biol***211**, 2989-3000.
**Gunther, M., Keppler, V., Seyfarth, A. and Blickhan, R.** (2004). Human leg design: optimal axial alignment under constraints. *J Math Biol* **48**, 623-646.
**Hancock, J. A., Stevens, N. A. and Biknevicius, A. R.** (2007). Whole-body mechanics and kinematics of terrestrial locomotion in the Elegant-crested Tinamou. Eudromia elegans. *Ibis* **149**, 605-614.
**He, J. P., Kram, R. and McMahon, T. A.** (1991). Mechanics of running under simulated low gravity. *J Appl Physiol***71**, 863-870.
**Heglund, N. C., Cavagna, G. A., Taylor, C. R.** (1982). Energetics and mechanics of terrestrial locomotion. III. Energy changes of the centre of mass as a function of speed and body size in birds and mammals. *J. Exp. Biol.* **97**, 41-56.
**Higham, T. E., Biewener, A. A. and Wakeling, J. M.** (2008). Functional diversification within and between muscle synergists during locomotion. *Biol Lett* **4**, 41-44.
**Hutchinson, J. R. and Allen, V.** (2009). The evolutionary continuum of limb function from early theropods to birds. *Naturwissenschaften* **96**, 423-448.
**Jenkins, P. A. and Weijs, W. A.** (1979). The functional anatomy of the shoulder in the Virginia opossum (Didelphis virginiana). *J Zool* **188**, 379-410.
**Kerdok, A. E., Biewener, A. A., McMahon, T. A., Weyand, P. G. and Herr, H. M.** (2002). Energetics and mechanics of human running on surfaces of different stiffnesses. *J Appl Physiol* **92**, 469-478.
**Kuitunen, S., Komi, P. V. and Kyröläinen, H.** (2002). Knee and ankle joint stiffness in sprint running. *Med sci sports exerc* **34**, 166-173.
**Lipfert, S. W., Günther, M., Renjewski, D., Grimmer, S. and Seyfarth, A.** (2012). A model-experiment comparison of system dynamics for human walking and running. *J TheorBiol* **292**, 11-17.
**Maus, H. M., Lipfert, S. W., Gross, M., Rummel, J. and Seyfarth, A.** (2010). Upright human gait did not provide a major mechanical challenge for our ancestors. *Nat Commun* **1**, 70.
**McMahon, T. A., Valiant, G. and Frederick, E. C.** (1987). Groucho running. *J Appl Physiol* **62**, 2326-2337.
**Moritz, C. T., Greene, S. M. and Farley, C. T.** (2004). Neuromuscular changes for hopping on a range of damped surfaces. *J Appl Physiol* **96**, 1996-2004.
**Muller, R. and Blickhan, R.** (2010). Running on uneven ground: leg adjustments to altered ground level. *Hum Mov Sci* **29**, 578-589.
**Muller, R., Grimmer, S. and Blickhan, R.** (2010). Running on uneven ground: leg adjustments by muscle pre-activation control. *Hum Mov Sci* **29**, 299-310.
**Nudds, R. L., Folkow, L. P., Lees, J. J., Tickle, P. G., Stokkan, K. A. and Codd, J. R.** (2011). Evidence for energy savings from aerial running in the Svalbard rock ptarmigan (Lagopus muta hyperborea). *Proc. R. Soc. Lond. B* **278**, 2654-2661.
**Nyakatura, J. A. and Andrada, E.** (2013). A mechanical link model of two-toed sloths: no pendular mechanics during suspensory locomotion. *Acta Theriol 58(1)*, 83-93.
**Nyakatura, J. A., Andrada, E., Grimm, N., Weise, H. and Fischer, M. S.** (2012). Kinematics and Center of Mass Mechanics During Terrestrial Locomotion in Northern Lapwings (Vanellus vanellus, Charadriiformes). *J Exp Zool A Ecol Genet Physiol* **317**, 580-594.

**Rubenson, J., Heliams, D. B., Lloyd, D. G. and Fournier, P. A.** (2004). Gait selection in the ostrich: mechanical and metabolic characteristics of walking and running with and without an aerial phase. *Proc. R. Soc. Lond. B* **271**, 1091-1099.

**Rubenson, J., Lloyd, D. G., Besier, T. F., Heliams, D. B., and Fournier, P. A.** (2007). Running in ostriches (*Struthio camelus*): three-dimensional joint axes alignment and joint kinematics. *J Exp Biol* **210**, 2548-2562. doi:10.1242/jeb.02792

**Rubenson, J., Lloyd, D. G., Heliams, D. B., Besier, T. F. and Fournier, P. A.** (2010). Adaptations for economical bipedal running: the effect of limb structure on three-dimensional joint mechanics. *J R Soc Interface* **8**, 740-755.

**Seyfarth, A., Geyer, H. and Herr, H.** (2003). Swing-leg retraction: a simple control model for stable running. *J Exp Biol* **206**, 2547-2555.

**Stoessel, A. and Fischer, M. S.** (2012). Comparative intralimb coordination in avian bipedal locomotion. *J Exp Biol* **215**, 4055-4069.

**Usherwood, J. R. and Hubel, T. Y.** (2012). Energetically optimal running requires torques about the centre of mass. *J R Soc Interface* **9**, 2011-2015.

**Winter, D. A.** (1995). Biomechanics and Motor Control of Human Movement. New York: John Wiley and Sons.

**Witte, H., Biltzinger, J., Hackert, R., Schilling, N., Schmidt, M., Reich, C. and Fischer, M. S.** (2002). Torque patterns of the limbs of small therian mammals during locomotion on flat ground. *J Exp Biol* **205**, 1339-1353.

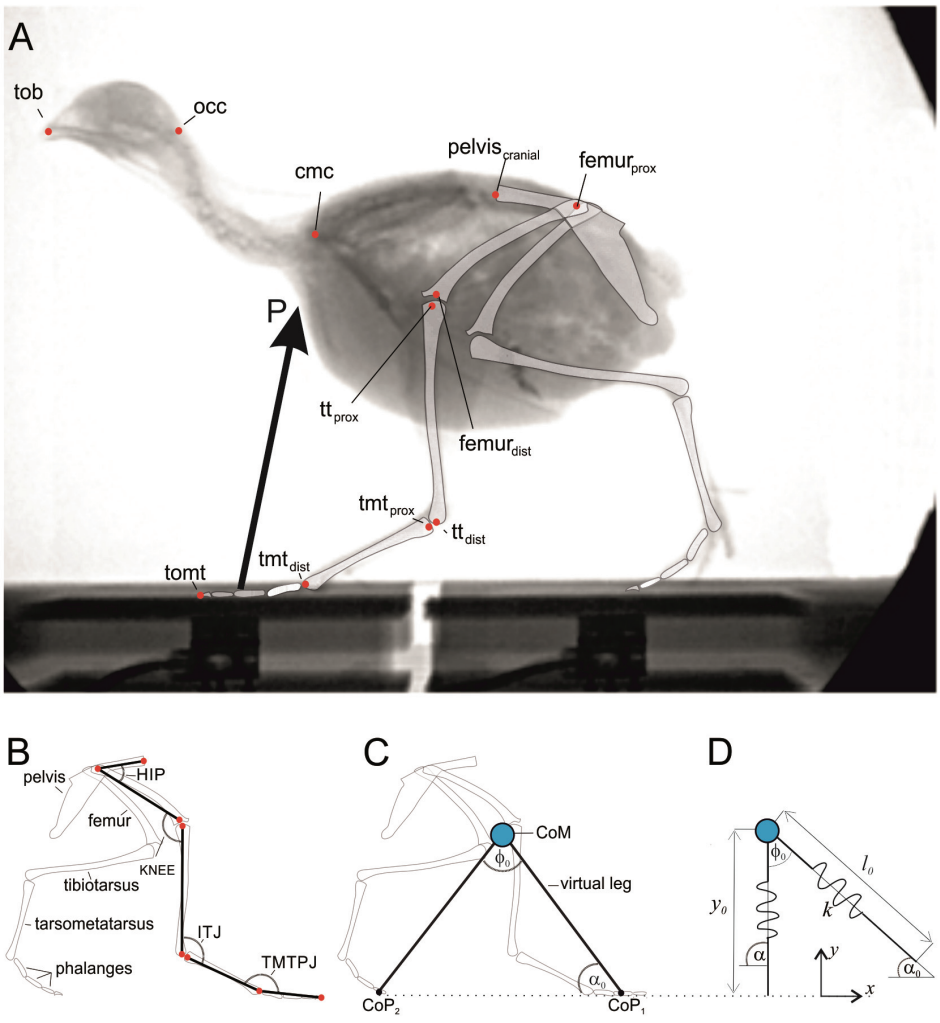


**Figure 1**. Latero-lateral X-ray projection of a quail traversing the two custom-built force plates to obtain single limb kinetic data. Schematic drawing superimposed to X-ray still image depicting all used landmarks (A) and two dimensional representation to measure joint angles (B). P: instantaneous ground reaction force vector; ITJ, intertarsal joint; TMTPJ, tarsometatarso-phalangeal joint; tob, tip of beak; occ, occiput; cmc, caudalmost cervical vertebrae; tomt, tip of middle toe. The TMTPJ was represented by one point ($tmt_{dist}$) due to the spatial resolution of the X-ray image. (C) Virtual legs at touch-down (segments $CoP_1$-CoM-$CoP_2$). $\alpha_0$: angle of attack, and $\phi_0$: aperture angle at touch-down. (D) Bipedal Spring Loaded Inverted Pendulum (BSILP) template. $k$: stiffness, $\alpha$: leg angle respect to the ground, $l_0$: rest length, $y_0$: initial high.

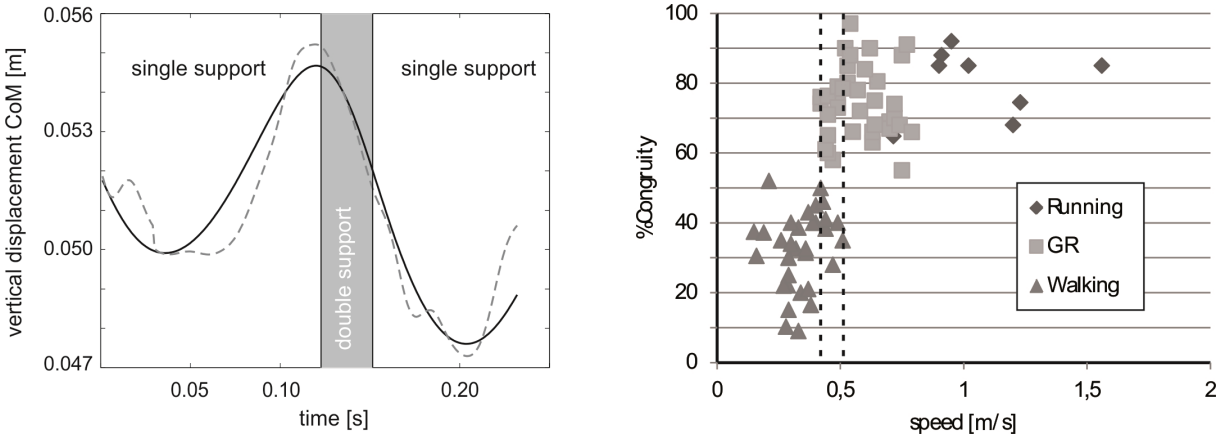


**Figure 2**. A) Estimation of vertical displacement of the CoM for a grounded running trial of a quail (grey dashed line: by combining kinematics and cadaveric information; black solid line: by using integration of GRF). B) %Congruity vs. speed. %Congruity was used to distinguish between walking and running gaits. We defined walking for %Congruity values < 50 and running for %Congruity values > 50. Trials with a % Congruity close to 50% were further analyzed to differentiate walking and running (shape of GRF, vertical speed change close to mid-stance, see methods). Vertical dashed lines depict overlapping speeds where walking and grounded running occur.

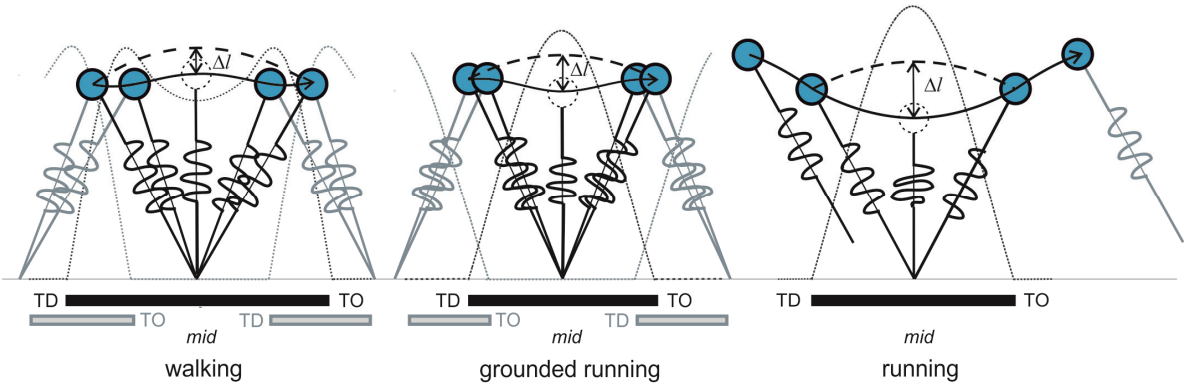


713
714

715 **Figure 3**. Estimating single-leg stiffness *k* during walking, grounded running and running, based on the BSLIP
716 template (black: leg 1, grey: leg 2). At touchdown (TD) and at take-off (TO) events, the "virtual leg" linking the
717 CoM with the CoP is equivalent to the rest length of a spring $l_0$; during stance, the virtual leg length is
718 compressed to exert the leg's GRF. The dashed arcs show the trajectory of $l_0$, the solid curves the trajectory of
719 the CoM, and the dotted curves represent the vertical component of the GRF. For all three gaits, the stiffness *k*
720 can be estimated, assuming linear behavior, as $k = GRF/\Delta l$. By choosing mid-stance (*mid*), only the vertical
721 component of the *GRF* and $\Delta l$ are needed to estimate it. Note that although stiffness is measured for single legs,
722 the model is bipedal for walking as well as for grounded running.

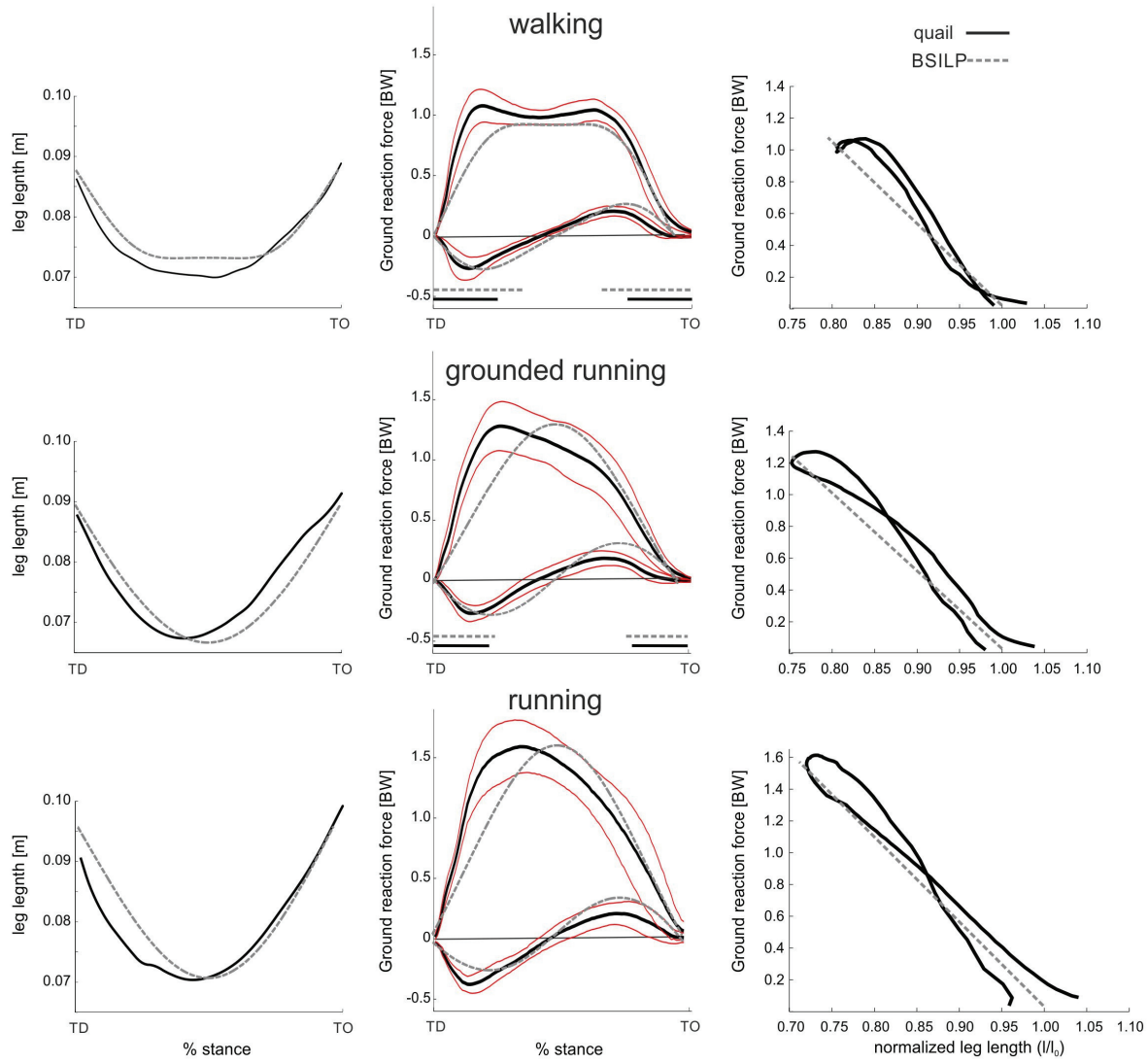


**Figure 4**. Global leg parameters during terrestrial locomotion of the quail vs. BSLIP simulation predictions. Solid lines represent experimental findings. Grey dashed lines BSLIP model. Leg length variation (left), vertical and anterior-posterior ground reaction forces (middle), and force-length plots (right) during walking (top), grounded running (middle) and running (bottom). The GRF and force-length plots are presented as mean (walking, n=32; grounded running, n=34; running, n=8). GRF graphs includes also ± 1s.d. Horizontal lines in the GRF graphs represent relative double support phases (walking and grounded running). For the force-length plots, resultant force is used. $l_0$ in the force-length plots refers to the mean value of $l_0$ for each gait (see table 2). Simulations parameters: walking, $v_{x0}$=0.34$m/s$, $\hat{k}$ = 5.8, $l_0$ = 0.087$m$, $E$ = 0.168$J$, $\alpha_0$ = 58°, grounded running: $v_{0x}$ = 0.59m/s, $\hat{k}$ =5, $l_0$ = 0.089 $m$, $E$ = 0.191$J$, $\phi_0$ = 65°, running: $v_{0x}$ = 1.06$m/s$, $\hat{k}$ = 6.2, $l_0$ = 0.096$m$, $E$ = 0.286$J$, $\alpha_0$ = 57°. Caution is needed when interpreting results of simulations for walking: a less compressed spring-leg at mid-stance would pronounce the vertical GRF's M-shape and simultaneously diminish the relative duration of double support phases.

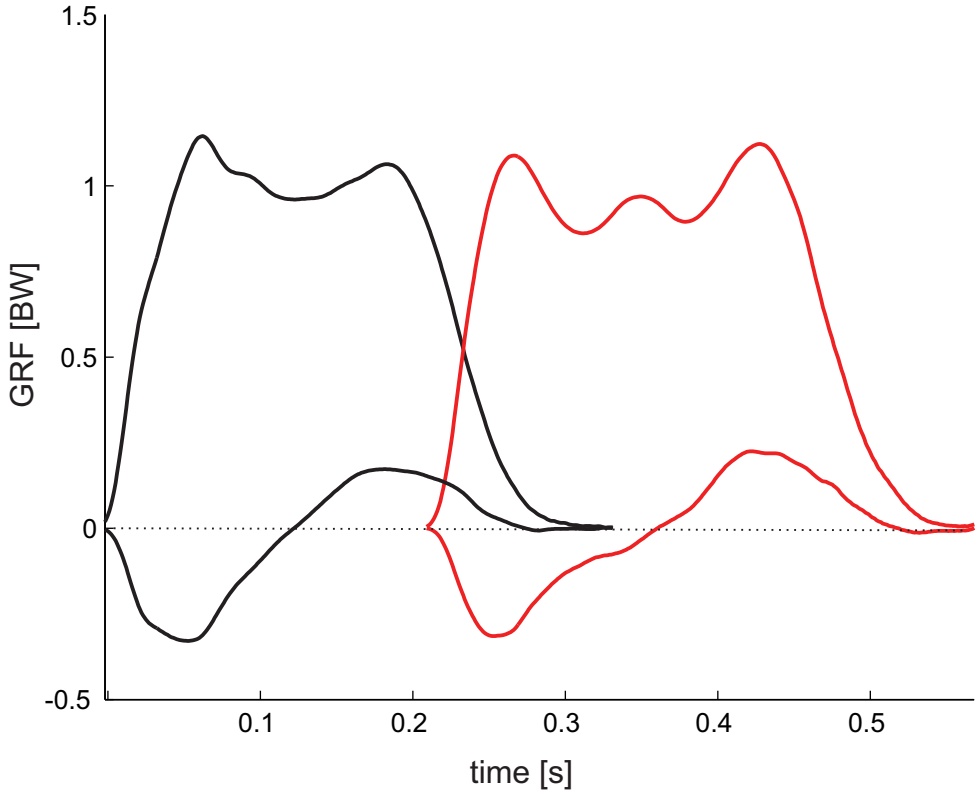


**Figure 5**. Vertical and anterior-posterior ground reaction forces obtained during slow walking. Note that vertical GFR obtained for the second stride show a three humped profile as predicted by the BSLIP model at slow speeds.

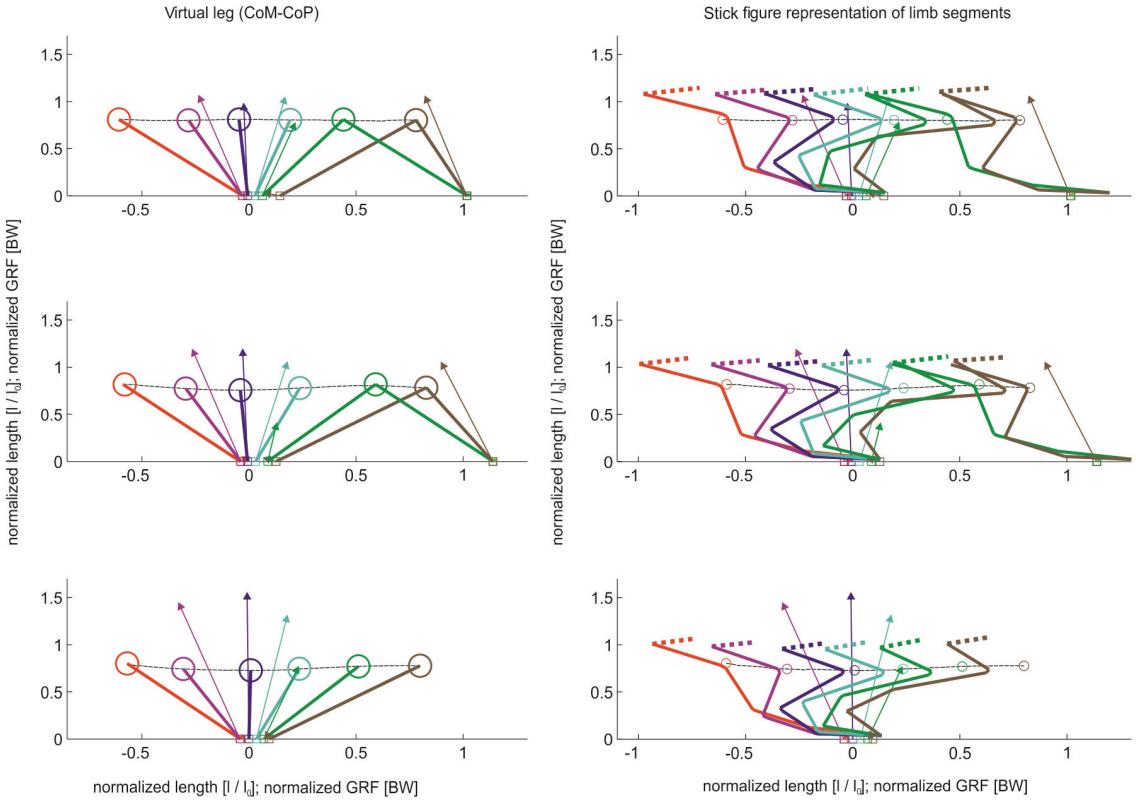


**Figure 6**. Virtual and stick figure representation of limb segments together with the orientation of the GRF during walking (top, mean of 32 strides), grounded running (middle, mean of 34 strides), and running (bottom, mean of 8 strides). Circles depict the position of the CoM. Segments were scaled by $l_0$ and GRF by body weight. Note that contrary to the (B)SLIP expectations, GRF are eccentric related to the virtual leg and the CoP is displaced cranially during stance.

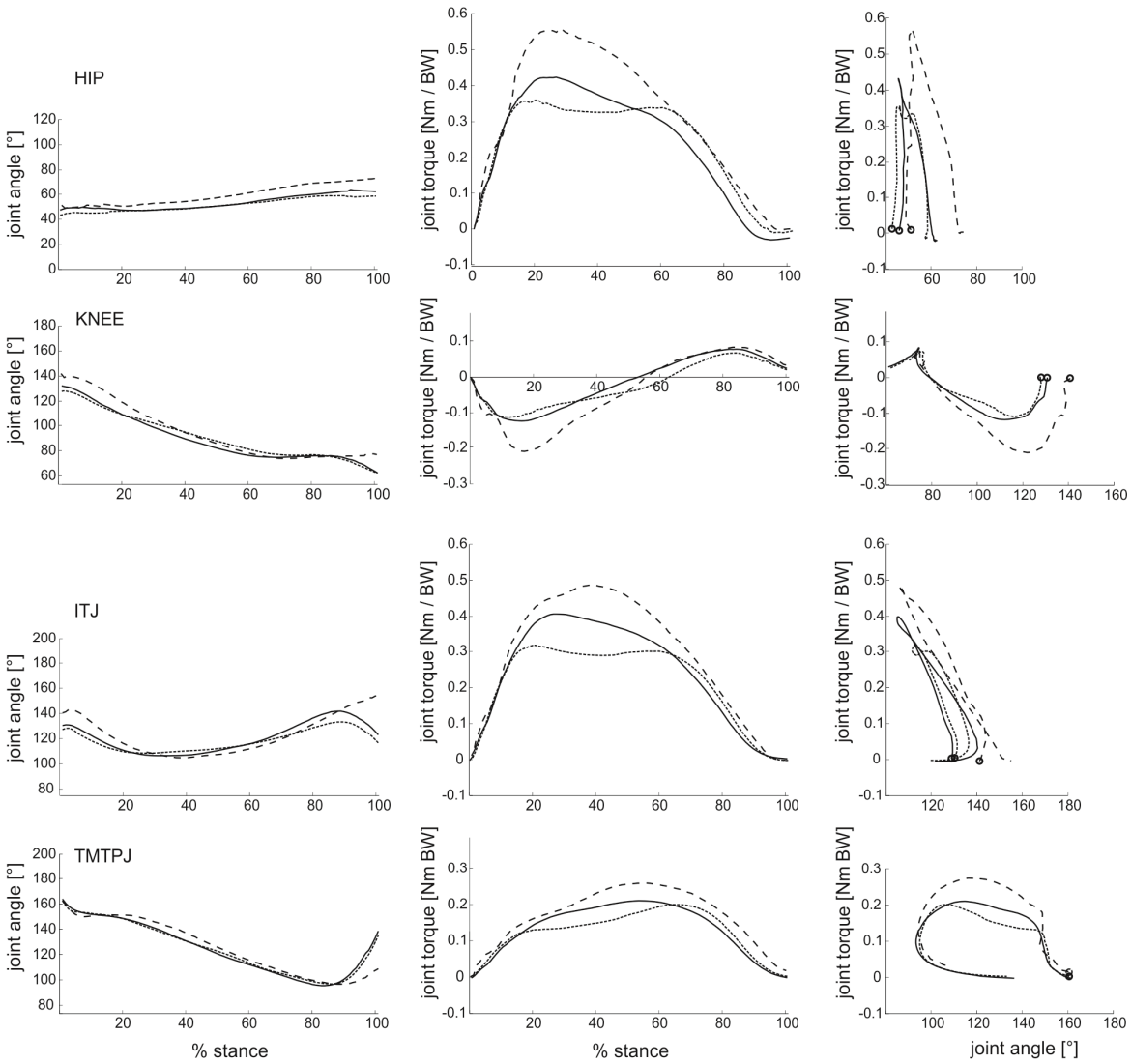


**Figure 7**. Local leg parameters (joint mechanics) during terrestrial locomotion of the quail (walking: dot-line, grounded running: solid line, running: dashed-line). Joint angles (left), joint torques (middle), torque-angle plots (right) over the course of the stance for the HIP, KNEE, ITJ, and TMTPJ. Displayed are mean values (walking: 32 strides, grounded running: 34 strides, running: 8 strides). Increasing joint angles indicate extension, and positive values in the torques plots represent extensor torques. Circles indicate touch-down.

768 **Table 1**: Limb element and body part parameters of subject 6. Relative position (from proximal) of the
769 element's CoM is given as percentage of overall length. *: value assumed; **: the CoM position of the
770 trunk is more ventral than the line between the pygostyl and caudalmost cervical vertebra; ***: due to
771 movements of the head relative to the trunk the length of the neck changes during locomotion.
772

| element | weight in g | % of total mass | length in cm | CoM position (% of total segment length) |
|---|---|---|---|---|
| trunk | 173.6 | 0.724 | 7.5 | 0.5, -0.307** |
| head | 7.5 | 0.031 | 4.4 | 0.328 |
| neck | 17.7 | 0.074 | variable*** | 0.32 |
| femur (thigh) | 11.1 | 0.046 | 4.1 | 0.483 |
| tibiotarsus | 7.1 | 0.029 | 5.18 | 0.35 |
| tarsometatarsus | 1.6 | 0.007 | 3.5 | 0.5* |
| toes | 0.6 | 0.003 | 3.9 | 0.5* |

773

774

**Table 2**: Gait related global leg parameters. $\hat{k}$ : dimensionless global leg stiffness; $l_0$. rest length; $\alpha_0$: angle of attack; $\phi_0$: aperture angle; $\psi$: dimensionless global leg compression; c.t. exp.: contact time in experimental quail data; c. t. sim.: contact time in simulation ; d. s. exp.: double support time in experimental quail data; d. s. sim.: double support time in simulation (mean ± 1 s.d.; p: significance t-test <0.05).

| parameter | walking | n | grounded running | n | running | n | p w. *vs* g.r. | p w. *vs* r. | p g.r. *vs* r. |
|---|---|---|---|---|---|---|---|---|---|
| $\hat{k}$ | 5.77 ±1.25 | 32 | 4.99 ± 0.67 | 34 | 6,15 ± 0.62 | 8 | 0.004 | 0.432 | <.001 |
| $l_0$ $[m]$ | 0.0872 ± 0.0087 | 32 | 0.0886 ± 0.007 | 34 | 0.0956 ± 0.009 | 8 | 0.793 | 0.036 | 0.022 |
| $\alpha_0$ [°] | 58 ± 3 | 32 | 56.7 ± 3.6 | 34 | 57.2 ± 3 | 8 | 0.277 | 0.54 | 0.74 |
| $\phi_0$ [°] | 57.1 ± 4 | 18 | 65.8 ± 5 | 21 | not defined | | <.001 | -- | -- |
| $\psi$ | 0.945 ± 0.04 | 32 | 1.2 ± 0.112 | 34 | 1.54±0.15 | 8 | <.001 | <.001 | <.001 |
| c. t. exp. $[s]$ | 0.31± 0.05 | 32 | 0.23± 0.05 | 34 | 0.124± 0.022 | 8 | <.001 | <.001 | <.001 |
| c. t. sim. $[s]$ | 0.253 | | 0.173 | | 0.121 | | | | |
| d. s. exp. $[s]$ | 0.08 ± 0.017 | 18 | 0.05 ± 0.013 | 21 | --- | | <.001 | | |
| d. s. sim. $[s]$ | 0.1 | | 0.041 | | | | | | |

783 **Table 3:** Gait related local leg parameters. Values presented are mean ±1 s.d. of maximal torques for
784 each joint and the rotational stiffness for the intertarsal joint (ITJ) at each gait . Torques are displayed
785 in Nm/Kg, and the rotational stiffness in Nm/Kg°. Gait related increment resp. decrement is shown in
786 %. t-test significance level $p < 0.05$.
787
788

| parameter | walking | grounded running | running | w. *vs* g.r. | w. *vs* r. | g.r. *vs* r. |
|---|---|---|---|---|---|---|
| Torque TMTPJ | 0.207± 0.05 | 0.221±0.036 | 0.261 ± 0.041 | 6.8 %<br>.23 | 26.1 %<br>.008 | 18.1 %<br>.009 |
| Torque ITJ | 0.343± 0.086 | 0.407± 0.054 | 0.503± 0.063 | 18.7 %<br>.001 | 46.7 %<br><.001 | 23.6 %<br><.001 |
| Torque knee | 0.129± 0.051 | 0.138± 0.037 | 0.223 ± 0.06 | 7 %<br>.44 | 72.9 %<br><.001 | 61.6 %<br><.001 |
| Torque hip | 0.399± 0.078 | 0.451± 0.061 | 0.581 ± 0,06 | 13 %<br>.004 | 45.6 %<br><.001 | 28.8 %<br><.001 |
| rot. stiffness ITJ | 0.014 ± 0.004 | 0.011 ± 0.002 | 0.011 ± 0.003 | -20%<br>0.01 | -20.7 %<br>0.096 | -0.9%<br>0.92 |

789
790